Original papers
Biological materials; nanomedicine, and novel technologies for clinical and medical applications

УДК 615.28 DOI: 10.17277/jamt-2025-10-03-236-246

Copper ferrite nanoparticles with antifouling activity

© Ekaterina A. Vornakova[a]✉, Valeria R. Chzhou[a], Olga V. Bakina[a], Ludmila Yu. Ivanova[a], Anastasia E. Yafaeva[a], Marat I. Lerner[a]

[a] *Institute of Strength Physics and Materials Science of Siberian Branch Russian Academy of Sciences, 2/4, Akademicheskii Av., Tomsk, 634055, Russian Federation*

✉ katya.vornakova@mail.ru

Abstract: Currently, metal ferrites are promising yet under-researched narrow band gap semiconductors for preventing biofouling. In the present study, nanoparticles with copper ferrites content of 55, 85 and 95 % were synthesized by electrical explosion of iron and copper wires in mixed oxygen and argon atmosphere. $CuFe_2O_4$ content was ranged by the wires diameter. According to the X-ray diffraction analysis, an increase of iron content in the twist led to an increase of copper ferrite phase up to 95 %. Copper oxide (I, II) and copper phases also were found in nanoparticles. The XRD data showed a uniform distribution of Cu and Fe in nanoparticles. Nanoparticles with $CuFe_2O_4$ content of 85 wt. % showed the highest efficiency in Congo red degradation reaction under visible light irradiation (decolorisation efficiency of 72 %). Nanoparticles (85 wt. % $CuFe_2O_4$) showed a high antibacterial activity against antibiotic resistant MRSA ATCC 43300 (bacteria growth reduction by 98.7 %). Moreover, NPs were active against *P. aeruginosa* biofilm, thus making them potential antibiofouling agents for water-contact items.

Keywords: copper ferrite; nanoparticles; photochemical activity; antibacterial activity; biofilms.

For citation: Vornakova EA, Chzhou VR, Bakina OV, Ivanova LYu, Yafaeva AE, Lerner MI. Copper ferrite nanoparticles with antifouling activity. *Journal of Advanced Materials and Technologies*. 2025;10(3):236-246. DOI: 10.17277/jamt-2025-10-03-236-246

Наночастицы феррита меди с противообрастающей активностью

© Е. А. Ворнакова[a]✉, В. Р. Чжоу[a], О. В. Бакина[a], Л. Ю. Иванова[a], А. Э. Яфаева[a], М. И. Лернер[a]

[a] *Институт физики прочности и материаловедения СО РАН, пр. Академический, 2/4, Томск, 634055, Российская Федерация*

✉ katya.vornakova@mail.ru

Аннотация: В настоящее время ферриты металлов являются многообещающим, но недостаточно исследованным классом узкозонных полупроводников для борьбы с биологическим обрастанием. В работе наночастицы, содержащие феррит меди ($CuFe_2O_4$) с массовой долей 55, 85 и 95 %, были получены при помощи электрического взрыва железной и медной проволок в смешанной атмосфере аргона и кислорода. Содержание $CuFe_2O_4$ варьировали диаметром проволок. По данным рентгенофазового анализа увеличение содержания железа в скрутке приводило к увеличению массовой доли феррита до 95 %. В частицах также обнаруживались фазы оксидов меди (I, II) и металлическая медь. Данные ЭДС анализа показали, что Cu и Fe распределены в частицах равномерно. В реакции разложения модельного красителя Конго красного установлено, что наночастицы, содержащие 85 масс. % $CuFe_2O_4$, обладали наибольшей фотохимической активностью (степень деколоризации 72 %) под действием видимого света. Наночастицы (85 масс. % $CuFe_2O_4$) продемонстрировали высокую антибактериальную активность в отношении устойчивого штамма MRSA ATCC 43300 (сокращение количества бактерий на 98,7 %). Кроме того, частицы продемонстрировали активность в отношении биопленок *P. aeruginosa,* что позволяет рассматривать их в качестве потенциальных противообрастающих агентов для изделий, контактирующих с жидкостями.

Ключевые слова: феррит меди; наночастицы; фотохимическая активность; антибактериальная активность; биопленки.

Для цитирования: Vornakova EA, Chzhou VR, Bakina OV, Ivanova LYu, Yafaeva AE, Lerner MI. Copper ferrite nanoparticles with antifouling activity. *Journal of Advanced Materials and Technologies*. 2025;10(3):236-246. DOI: 10.17277/jamt-2025-10-03-236-246

1. Introduction

Currently, the problem of biofouling caused by biofilms is of serious concern in healthcare, water treatment and marine structures [1]. Biofouling of surfaces, especially fouling of ships [2] and medical implants, catheters, hemodialyzers, biosensors, respirators [3] remains a serious problem. In practice, copper (I) oxide-based substances are used to combat biofouling. Protective compounds are used to paint the surfaces of ships, fishing nets, sensors, etc. [4]. However, Cu_2O-based compounds have low efficiency and, therefore large amounts (at least 40 % by weight) of copper (I) oxide is used, which can harm marine organisms [5]. With long-term use of paints containing Cu_2O, some microorganisms developed resistance to them [6]. Thus, there is a need to develop alternative antifouling additives to replace traditional toxic biocides. Such additives may become competitive and effective means for combating biofouling.

Due to their developed surface and high activity, nanoparticles (NPs) are widely used in coatings to suppress corrosion, fouling and scratching of metal materials [7]. The most promising for preventing biofouling are metal NPs (Cu, Ag, Zn, Ti, etc.), their compounds and complex nanostructures metal-metal oxide, metal oxide-metal oxide, etc. [8]. A promising class of narrowbandgap semiconductors is ferrites – oxide compounds with the chemical formula $MeFe_2O_4$, containing Fe^{3+} and a cation of another metal (Cu, Zn, Co, etc.). Ferrites are characterized by absorption in the visible region, tunable optoelectronic properties, and high chemical and mechanical stability [9]. $CuFe_2O_4$ nanoparticles are one of the most promising spinel ferrites due to their magnetic properties, low toxicity, and photochemical activity under the exposure to visible light [10]. Copper ferrite nanoparticles have a band gap of about 1.8 eV. The absorption band edge may shift slightly depending on the synthesis method, the presence of impurities, the carrier concentration, the crystallite size, and the lattice deformation. Such NPs can be easily separated by magnetic separation for recovery and replacement in the reaction mixture [11]. $CuFe_2O_4$ NPs demonstrate antibacterial activity against *Escherichia coli, Staphylococcus aureus* [12], methicillin-resistant *Staphylococcus aureus* (MRSA) [13], *Bacillus cerus* [14]. The authors [15] confirmed the antibacterial activity of $CuFe_2O_4$ NPs in the absence of toxicity to erythrocyte cells. In [16], it was shown that the addition of 6 % $CuFe_2O_4$ NPs to the zeolite framework allowed for 98 % inhibition of *Escherichia coli* bacteria growth on the surface even after 7 recirculation cycles.

Various methods are used to synthesize $CuFe_2O_4$ NPs, including chemical precipitation, hydrothermal synthesis, sublimation drying, microemulsion synthesis, and sol-gel synthesis [17]. Of greatest interest are the methods for synthesizing NPs based on the self-assembly of target phase clusters under highly non-equilibrium conditions in a gas atmosphere. Such methods are relatively simple, have no synthesis by-products, are scalable, and do not use harmful solvents.

In this paper, electrical explosion of wires (EEW) – copper and iron – in an oxygen-containing atmosphere was used to obtain $CuFe_2O_4$ NPs. Previously we had prepared $CuO/CuFe_2O_4$ NPs with a ferrite phase content of 10 % by weight [18]. In order to increase the proportion of this phase, the iron content in the exploded wires was increased in this paper. The synthesized NPs were characterized by a set of physicochemical methods of analysis, and examined for photochemical, antimicrobial, and biofouling activity. The results showed that the NPs exhibit high antibacterial activity and are effective in combating biofilms.

2. Materials and Methods

2.1. Initial materials

Nanoparticles with different $CuFe_2O_4$ content were prepared by electric explosion of copper and iron wires twisted together in a mixed oxygen and argon atmosphere, the oxygen content of which was 20 vol. %, using the UDP-2 setup (Advanced Powder Technologies LTD, Tomsk, Russia). The $CuFe_2O_4$ content in the nanopowder was regulated by the diameter of the metal wires. The EEW parameters, such as wire diameter d_w, wire length l_w, capacitor capacitance C, discharge voltage U_0, are given in Table 1. The numbers in brackets correspond to the content of the ferrite phase in the NP. Photographs of the prepared samples are shown in Fig. 1.

Table 1. $CuFe_2O_4$ NP synthesis parameters

Sample	Wire material	d_w, mm	l_w, mm	N, at. %	C, μF	U_0, kV
$CuFe_2O_4$ (95 %)	Fe	0.3	90	69.8	3.2	24
	Cu	0.2		30.2		
$CuFe_2O_4$ (85 %)	Fe	0.2	60	49.9	3.2	28
	Cu	0.2		50.1		
$CuFe_2O_4$ (55 %)	Fe	0.2	75	30.2	3.2	33
	Cu	0,3		69.,8		

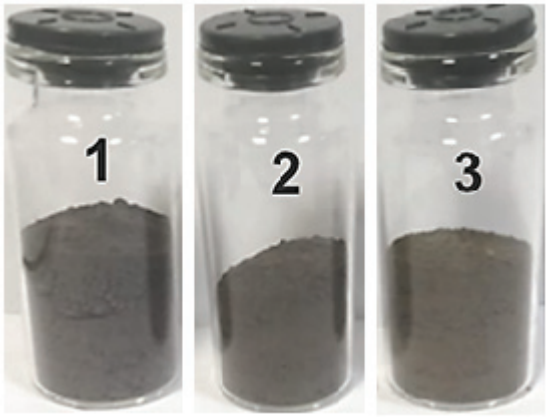

Fig. 1. Photos of NPs: 1 − $CuFe_2O_4$ (95 %); 2 − $CuFe_2O_4$ (85 %); 3 − $CuFe_2O_4$ (55 %)

2.2. Determination of photochemical, antibacterial and antifouling activity of nanoparticles

The photochemical activity of NPs was studied in the reaction of decomposition of the model dye Congo red. For this purpose, 0.01 g of nanoparticles was added to 50 mL of the dye with a concentration of 10 mg·L^{-1}. The resulting suspension was dispersed in an ultrasonic bath (VU-09-"Ya-FP"-03, Russia) for 15 min, after which the solution was constantly stirred in the dark for 60 min to achieve adsorption-desorption equilibrium in the system. Then the suspension was irradiated for an hour with visible radiation with a wavelength of λ = 550 nm, generated by a xenon lamp (OLKs-150M, Russia). Every 10 min, a sample was taken from the solution and the optical density of the supernatant was measured on an SF-2000 spectrophotometer (OKB Spektr, Russia) at the wavelength of maximum absorption (500 nm).

The degree of dye degradation was calculated using the formula:

$$\%D = \frac{C_0}{C_0 - C_t} 100\ \%, \qquad (1)$$

where C_0 is initial concentration of dye, mg·L^{-1}; C_t is concentration of dye after irradiation, mg·L^{-1}.

The antibacterial activity of $CuFe_2O_4$ nanoparticles was studied against the MRSA ATCC 43300 strain. The growth of the bacterial culture in the control solution and in the solution with $CuFe_2O_4$ nanoparticles was compared. For the control solution, bacteria were cultured in the Mueller-Hinton broth nutrient medium (Research Center of Pharmacology, Russia). The final concentration of bacteria was brought to 105 CFU (colony forming unit)/ml by serial dilutions according to MUK Instructions 4.2.1890-04. The solution with nanoparticles was prepared by introducing $CuFe_2O_4$ NPs (512 μg·mL^{-1}) into the previously prepared bacterial suspension. All solutions were incubated in a thermostat for (12 ± 1) h at (37 ± 1) °C. After the incubation time, the solution samples were additionally diluted 10, 100 and 1000 times with a buffer medium (saline solution), the resulting suspension was placed on 90 mm diameter Petri dishes with Mueller-Hinton agar medium (NICF, Russia) and incubated for (24 ± 3) h at (37 ± 1) °C. Antibacterial activity was measured using the formula:

$$R = \frac{\bar{x}(k) - \bar{x}}{\bar{x}(k)} 100\ \%, \qquad (2)$$

where $\bar{x}(k)$ is average number of colonies grown in the test solution; $\bar{x}$ is average number of colonies grown in the solution with nanoparticles.

The antifouling activity of nanoparticles was studied according to the method described in ISO 4768:2023 "Measurement method of anti-biofilm activity on plastic and other non-porous surfaces", using the bacterial strain *Pseudomonas aeruginosa* ATCC 27853. The choice of the bacterial strain was due to its wide application for assessing antifouling activity, difficulty in treatment, and ability to quickly form biofilms that cover them [19].

A bacterial suspension with a concentration of 107 CFU/mL with the addition of $CuFe_2O_4$ NPs (512 μg·mL^{-1}) was placed in a 96-well sterile plate (TPP, Switzerland) and incubated at 37 °C for 24 h. Bacterial suspension without NPs was used as a control. Bacterial growth was monitored over time using optical density on a plate spectrophotometer (Thermo Scientific Multiscan FC, China). Then the contents of the plate wells were drained and washed with distilled water, and the biofilms were fixed with gentian violet dye (0.1 %), followed by rinsing with an ethanol solution (95 % by weight). The color intensity of the rinsing fluid was estimated by optical density on a spectrophotometer. Antifouling activity (B) against biofilm was calculated using the formula:

$$B = \frac{OD(k) - OD}{OD(k)} 100\ \%, \qquad (3)$$

where $OD(k)$ is the value of the average optical density in the test wash liquid; OD is the value of the average optical density in the wash liquid of the tested sample.

2.3. Analytical methods

The morphology and elemental composition of the NPs were determined using a JEM-2100 transmission electron microscope (JEOL, Japan) with an integrated X-Max energy-dispersive X-ray spectroscopy system (Oxford Instruments, UK). The phase composition of the NPs was analyzed by X-ray phase analysis (XRD) using an XRD 6000 diffractometer (Shimadzu Corporation, Japan), with CuKα radiation at 40 kV and 30 mA in scanning mode in the 2θ angle range from ~ 20° to 80° with a step of 0.02°, and an exposure of 1 s. Qualitative phase analysis was performed using the PDF-2 Release 2014 powder diffraction file database. The size distribution of NPs and NP agglomerates was determined using the sedimentation method with a CPS DS24000 disk centrifuge (CPS Instruments, USA). The specific surface area was measured by nitrogen thermal desorption using a specific surface analyzer (Sorbtometer-M, Russia). The specific surface area was determined using the Brunauer-Emmett-Teller (BET) equation using the instrument software. The surface composition was studied using X-ray photoelectron spectroscopy (SPECS Surface Nano Analysis GmbH, Berlin, Germany). Zeta potential measurements were performed in deionized water at 25 °C and pH from 5 to 11 on a Zetasizer Nano ZSP equipped with an MPT-2 autotitration device (Malvern Instruments Ltd, UK) using Zetasizer software.

3. Results and Discussion

During an electrical explosion of copper and iron wires, pairs and clusters of metals are formed, which are oxidized and, due to self-assembly, combine into NPs [20]. Since nanoparticles are formed in a medium of a mixture of inert gas and oxygen, the presence of undesirable impurities at the phase boundary is excluded, as in chemical methods of forming nanoparticles [21]. Self-assembly of clusters into NPs occurs under conditions of rapid cooling, which allows stabilizing potentially active nanoparticles with a non-stoichiometric composition [22].

According to the phase diagram of Cu and Fe metals in an oxygen-containing atmosphere (Cu–Fe–O system), the following phases can be formed depending on the metal ratio: CuO, Cu_2O, $CuFeO_2$, $CuFe_2O_4$, Fe_3O_4, FeO [23]. The results of X-ray phase analysis showed that the main phase is the copper ferrite phase $CuFe_2O_4$ (PDF Card No. 060545). The phases CuO (PDF Card No. 440706), Cu_2O (PDF Card No. 351091), Cu (PDF Card No. 031005) are also present. The Fe phase was not detected, indicating complete oxidation of the metal by oxygen (Fig. 2).

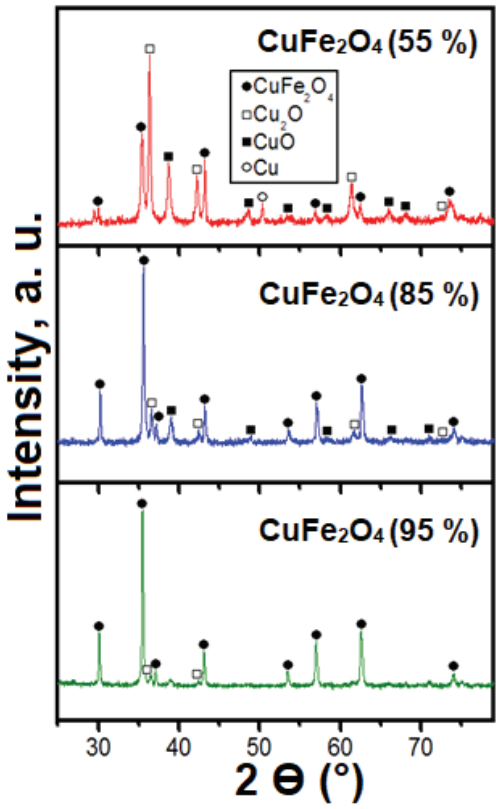

Fig. 2. XRD-patterns of the $CuFe_2O_4$ nanoparticles

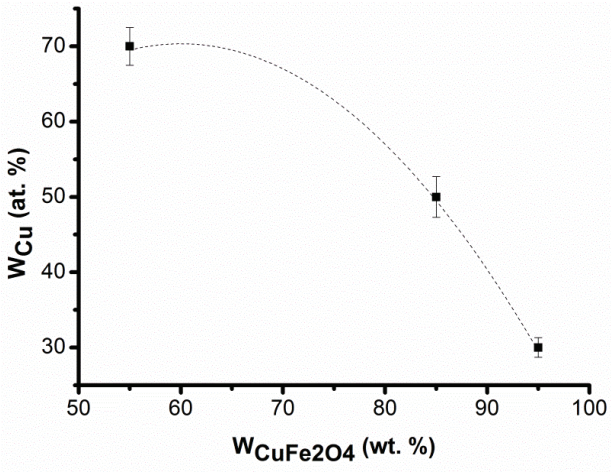

Fig. 3. $CuFe_2O_4$ mass ratio in NPs in dependence of Cu content

The crystal structure of spinel is a face-centered cubic packing formed by O^{2-} anions, Cu^{2+} and Fe^{3+} cations located in the voids. The diffraction peaks at 2θ angles of about 30.15°, 35.52°, 43.18°, 53.60°, 57.12°, 62.73° and 74.25° were identified as the (220), (311), (400), (422), (511), (440) planes of the cubic structure of $CuFe_2O_4$ spinel. This is confirmed by the data given in [24].

The diffraction peaks at 36°, 42.5° and 74° belong to the Cu_2O phase, and the peaks at 39° and 71° correspond to the CuO phase. The content of the ferrite phase was estimated by calculation based on the stoichiometry of this chemical compound, taking into account that all the iron was consumed in the synthesis of this compound. It was found that the content of the $CuFe_2O_4$ phase is inversely proportional to the copper content in the exploded twisted wire (Fig. 3).

Transmission electron microscopy showed that all particles were nearly spherical in shape; the smallest particles had weak faceting, while Cu, Fe and O were distributed uniformly in the particles (Fig. 4).

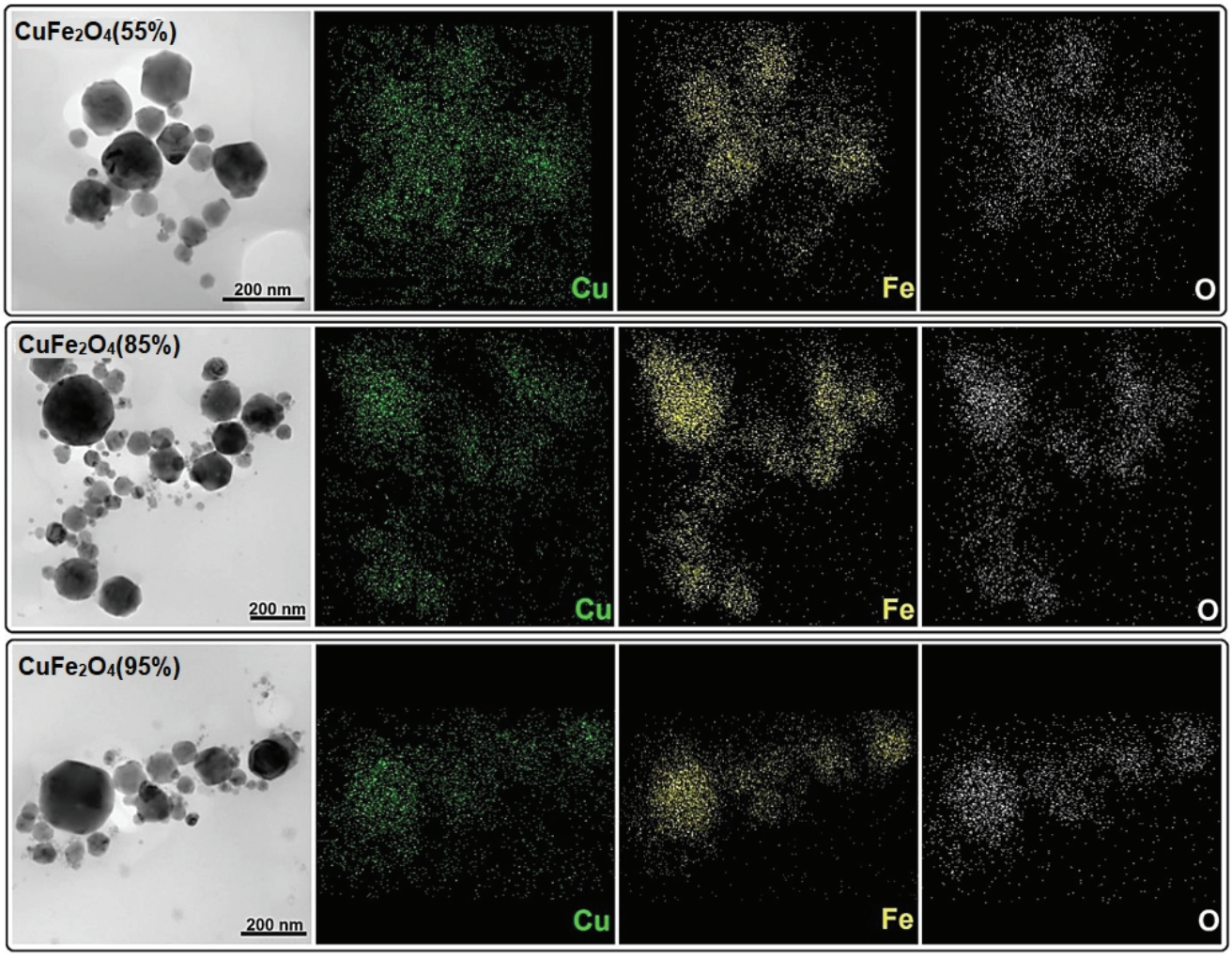

Fig. 4. TEM-images and EDX-analysis of $CuFe_2O_4$ nanoparticles

An increase in the $CuFe_2O_4$ phase content resulted in an increase in the specific surface area (from (3.2 ± 0.4) to (6.9 ± 0.2) $m^2 \cdot g^{-1}$), which is associated with an increase in the number of smaller agglomerates (the agglomerate size decreased from 0.66 to 0.49 μm). A study of the sizes of NP agglomerates by the sedimentation method (Fig. 5) showed a bimodal distribution with maxima at 30–50 and 100–200 nm. Based on the TEM results, the first maximum corresponds to the sizes of NPs, and the second to the sizes of particles and their agglomerates.

The effect of the medium pH on the NP charging properties was assessed by the change in the zeta potential (Fig. 6). For all particles, the zeta potential changes from (48 ± 2) mV in an acidic medium to (-35 ± 3) mV in an alkaline medium. In media with a physiological pH value (7.2), all nanoparticles were charged positively. The isoelectric point for a suspension of $CuFe_2O_4$ NPs (55 %) was 9.38; for $CuFe_2O_4$ (85 %) nanoparticles – 9.19; for $CuFe_2O_4$ (95 %) nanoparticles – 8.42. The shift of the isoelectric point towards lower pH values with an increase in the content of the $CuFe_2O_4$ phase is associated with a change in the composition of the NP surface. An increase in the content of copper oxide in NPs leads to an increase in its content on the surface.

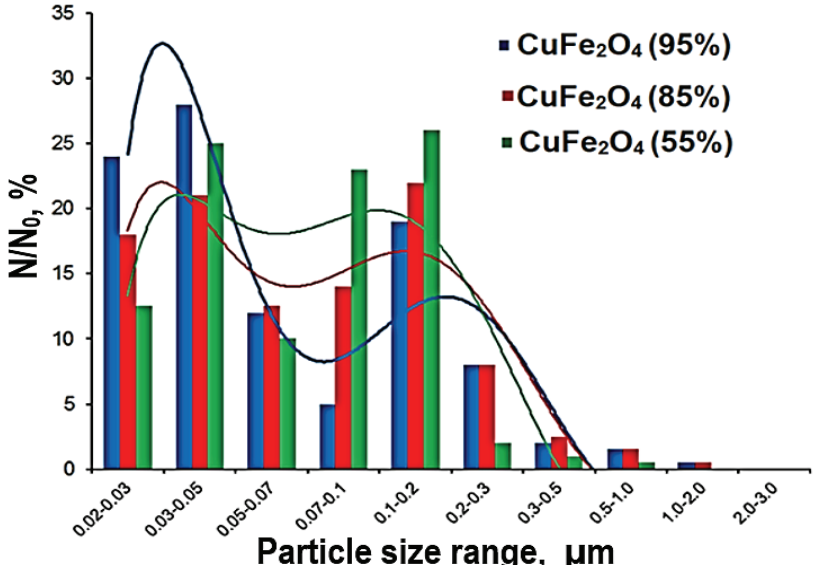

Fig. 5. Particle and agglomerate size distribution of $CuFe_2O_4$ NPs in an aqueous suspension

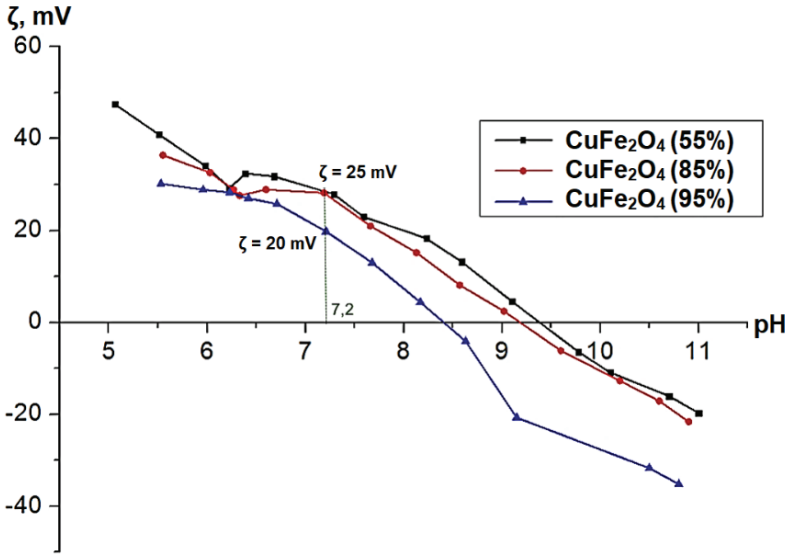

Fig. 6. $CuFe_2O_4$ NPs zeta potential dependence on the pH

Figure 7*a* shows typical spectra of Cu 2*p* NPs using $CuFe_2O_4$ (95 %) – 8.42 as an example. As is known, the Cu 2*p* spectrum is a Cu $2p_{3/2}$ – – Cu $2p_{1/2}$ doublet, the integral intensities of the components of which are related as 2 : 1. The spin-orbit splitting (the difference in the binding energies of Cu $2p_{3/2}$ and Cu $2p_{1/2}$Cu $2p_{3/2}$) is 19.9 eV. The shape of the spectrum indicates that copper is in the Cu^{2+} state, since there is a characteristic intense "shake-up" satellite in the region of high binding energies, usually observed for copper in the Cu^{2+} state [25, 26]. The integral intensity of the "shake-up" satellite in the CuO spectrum, for example, reaches 55 % of the intensity of the main line Cu $2p_{3/2}$ [27]. In the spectra of Cu^{1+} compounds, as well as in the spectrum of metallic copper, the "shake-up" satellite peaks are absent.

The Fe 2*p* spectra of the studied samples are shown in Fig. 7*b*. As can be seen, the Fe 2*p* spectra are the Fe $2p_{3/2}$ – Fe $2p_{1/2}$ doublet, the integral intensities of the components of which are related as 2 : 1. As a rule, to determine the state of iron, both the position of the main Fe $2p_{3/2}$ line and the shape of the Fe 2*p* spectrum are used, namely the intensity and relative position of the shake-up satellite lines caused by the manifestation of multielectron processes. The position and intensity of the shake-up satellite line depends on the chemical state of iron. In the case of the studied samples, the Fe $2p_{3/2}$ spectra are a peak with a binding energy in the region of 710.8 eV, while a shake-up satellite is observed, located 8.7 eV from the main peak. According to the literature data, iron in the composition of copper ferrite is characterized by Fe $2p_{3/2}$ binding energy values at 710.1 and 712.0 eV [28], with the "shake-up" satellites located at 5.7, 8.5 and 8.8 eV from the main Fe $2p_{3/2}$ peak. The high binding energy value and the presence of "shake-up" satellites allow us to state that iron in these samples is in the Fe^{3+} state.

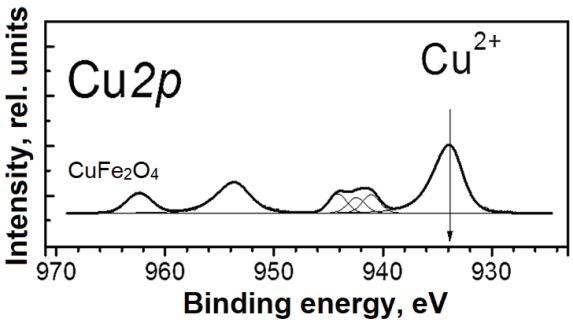

(a)

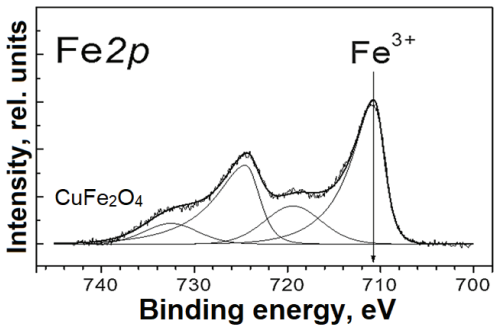

(b)

Fig. 7. X-ray photoelectron spectra of Cu 2*p* (*a*) and Fe 2*p* (*b*) for $CuFe_2O_4$ NPs. The spectra were normalized by the integral intensity of the peaks corresponding to the metals included in the NPs

One of the mechanisms of antifouling and antimicrobial action of NPs is generation of reactive oxygen species (ROS) due to radicals (•OH) and ($•O_2^-$), which damage the bacterial membrane, oxidize proteins and DNA and lead to cell death [29]. To study the possibility of ROS generation by $CuFe_2O_4$ NPs, their photochemical activity was studied in the decolorization reaction of the model dye Congo red under the influence of visible light. The choice of the dye was due to its resistance to light and natural decomposition, high carcinogenicity and presence in wastewater as textile waste [30]. The results obtained are presented in Fig. 8.

The studied nanoparticles showed different photocatalytic activity in decomposing the dye depending on the composition of the particles. A comparative assessment of the obtained results with published data is given in Table 2.

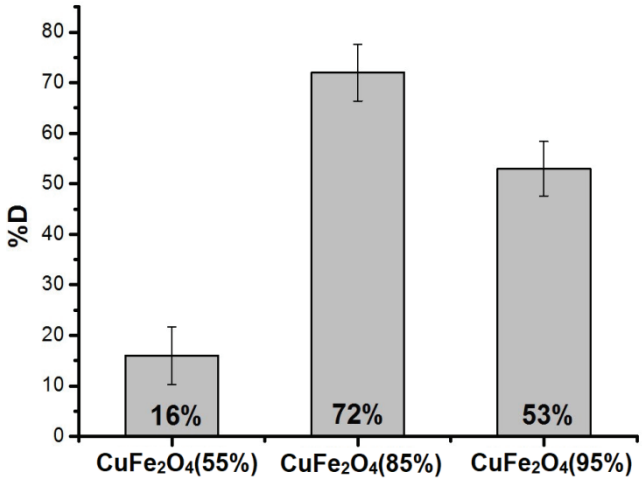

Fig. 8. $CuFe_2O_4$ NPs photochemical activity in Congo Red degradation reaction

Table 2. Comparative assessment of the photochemical activity of copper-containing ferrite nanoparticles during the decomposition of Congo red

Sample code	Synthesis method	Decomposition conditions	Decolorization, %	References
Copper ferrite nanocomposite (CFN)	Solvothermal synthesis	UV, 120 min	96.19	[31]
$Co_{1-x}Cu_xFe_2O_4$	Combustionmethod	Visiblelight, 90 min	71.37	[32]
$Ni_{0.6}Cu_{0.4}Ce_xFe_{2-x}O_4$	Chemical precipitation	Visiblelight, 120 min,	84.51	[33]
$CuFe_2O_4$	Sol-gelsynthesis	UV, 100 min	55	[34]
$Cu_{0.5}Fe_{1.5}Mn_{0.5}O_4$			79.1	
$Co_{0.4}Mg_{0.4}Cu_{0.2}Fe_{1.9}Cr_{0.1}O_4$	Sol-gelsynthesis	UV, 160 min	84	[35]
$Cu_{0.1}Zn_{0.9}Fe_2O_4$	Chemical precipitation	Visiblelight, 105 min	70	[36]
$ZnO–CuFe_2O_4$	Chemical precipitation	Visiblelight, 120 min	82	[37]
$CuFe_2O_4$ (85 %)	EEW	Visiblelight, 60 min	72	This paper

The possible mechanism of dye decomposition by copper ferrite has been described in detail in a large number of works, for example [38], and can be represented as the following reactions (1) – (4):

$$CuFe_2O_4 + h\nu \rightarrow e^- + h^+; \quad (1)$$

$$CuFe_2O_4\,(e^-) + O_2 \rightarrow \bullet O_2^-; \quad (2)$$

$$CuFe_2O_4\,(h^+) + H_2O \rightarrow \bullet OH; \quad (3)$$

$$\text{Congo red} + \bullet O_2^-/\bullet OH = \text{dye decolorization}. \quad (4)$$

When exposed to visible light, electrons in $CuFe_2O_4$ are excited and move from the valence band to the conduction band. These electrons can react with oxygen dissolved in water, forming the superoxide radical $\bullet O_2^-$. The holes formed in the valence band react with water molecules, forming the hydroxyl radical •OH. The resulting ROS interact with the dye molecules, which undergo decolorization to form H_2O, CO_2 and other mineral acids (decomposition products). With an increase in the copper content in the samples, the ability of ferrites to generate ROS decreases, as does their photocatalytic activity. $CuFe_2O_4$ NPs (55 %) practically did not lead to decolorization of the dye during 60 min of exposure (the degree of decolorization is about 16 %). This effect is an indirect evidence of an increase in the copper oxide content on the surface of the nanoparticles and a decrease in the $CuFe_2O_4$ content. With an increase in the copper content in the sample, the content of Cu_2O and CuO oxidesthat do not have photochemical activity increases.

Studies of the antibacterial activity of $CuFe_2O_4$ nanoparticles in the concentration range of 16−1024 μg·mL^{-1} showed that at a concentration of 512 μg·mL^{-1}, the $CuFe_2O_4$ (85 %) sample has a more pronounced antibacterial activity compared to other NPs, since the reduction in the amount of microorganism growth was on average 98.7 % (Table 3). This correlates with the results of the photocatalytic activity of the particles (Fig. 8). The high value of antibacterial activity can be associated with the fact that $CuFe_2O_4$ (85 %) nanoparticles more effectively generate hydroxyl and superoxide radicals, which are capable of disrupting the integrity of the bacterial cell membrane, which subsequently leads to its death.

Biofouling studies were performed on samples of $CuFe_2O_4$ (85 %) and $CuFe_2O_4$ (95 %) nanoparticle powder, which demonstrated the best antimicrobial efficiency. At the end of the incubation time, the optical density of the suspensions containing NPs had

Table 3. Antibacterial activity of $CuFe_2O_4$ nanoparticles

NPs	% reduction in MRSA ATCC 43300 bacteria after exposure to particles
$CuFe_2O_4$ (95 %)	95.2 ± 0.7
$CuFe_2O_4$ (85 %)	98.7 ± 3.2
$CuFe_2O_4$ (55 %)	62.4 ± 4.2

*R** – Reduction in microorganisms, %.

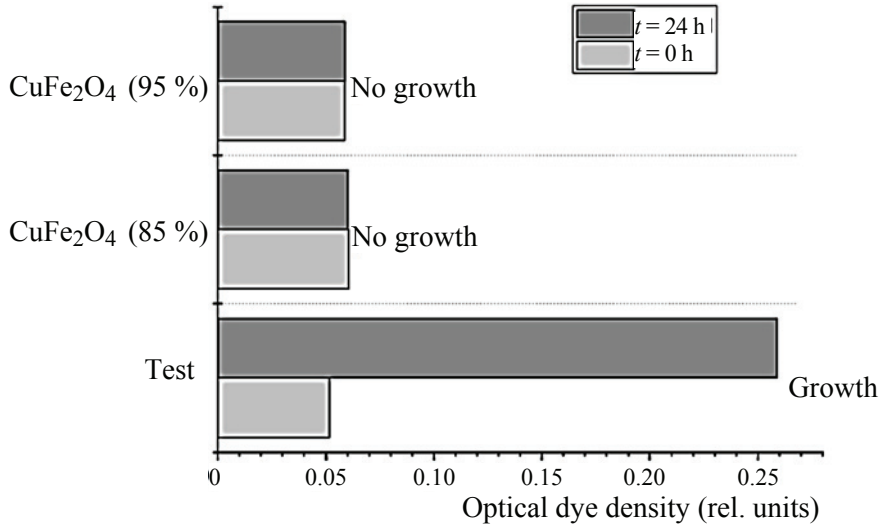

Fig. 9. *P. aeruginosa* biofilm growth inhibition study

a value close to the optical density at the beginning of the experiment, which indicated the suppression of *P. aeruginosa* bacteria growth by nanoparticles at a concentration of 512 μg·mL^{-1}. The results of wipe tests showed active formation of *P. aeruginosa* biofilms on the bottom of the polystyrene plate. In the presence of NPs, the antifouling activity reached 88 and 75 % for $CuFe_2O_4$ (85 wt. %) and $CuFe_2O_4$ (95 wt. %) NPs, respectively (Fig. 9).

4. Conclusion

In this study, nanoparticle samples with copper ferrite $CuFe_2O_4$ content of 55, 85 and 95 % by weight were prepared by combined electrical explosion of copper and iron wires in an oxygen-containing atmosphere. Regardless of the composition, the particles had a close to spherical shape and a bimodal distribution of agglomerates by size with distribution maxima in the range of 30–50 and 100–200 nm. Nanoparticles at a pH close to the physiological environment had a positive zeta potential, which promotes their adhesion to negatively charged bacterial cells. $CuFe_2O_4$ (85 wt. %) nanoparticles demonstrated the highest efficiency in the reaction of decomposition of the model dye Congo red: after 60 min of irradiation with visible light, the degree of decolorization of the dye reached 72 %, while for $CuFe_2O_4$ (95 wt. %) and $CuFe_2O_4$ (55 wt. %) NPs it was 53 % and 16 %, respectively. The resulting particles had antibacterial activity against MRSA and antifouling activity against *P. aeruginosa* biofilms.

5. Funding

The study was carried out as part of the state project of the Institute of Strength Physics and Materials Science SB RAS, topic FWRW-2022-0002.

6. Conflict of interest

The authors declare no conflict of interest.

References

1. Vuong P, McKinley A, Kaur P. Understanding biofouling and contaminant accretion on submerged marine structures. *npj Materials Degradation*. 2023;7(1):50. DOI:10.1038/s41529-023-00370-5

2. Qian PY, Cheng A, Wang R, Zhang R. Marine biofilms: diversity, interactions and biofouling. *Nature Reviews Microbiology*. 2022;20(11):671-684. DOI:10.1038/s41579-022-00744-7

3. He Z, Yang X, Wang N, Mu L, et al. Anti-biofouling polymers with special surface wettability for biomedical applications. *Frontiers in Bioengineering and Biotechnology*. 2021;9:807357. DOI:10.3389/fbioe.2021.807357

4. Ding T, Xu L, Liu X, Ma L, et al. A Cu_2O-based marine antifouling coating with controlled release of copper ion mediated by amphiphilic PLMA-b-PDMAEMA copolymers. *Progress in Organic Coatings*. 2022;170:107003. DOI:10.1016/j.porgcoat.2022.107003

5. Li H, Luo S, Zhang L, Zhao Z, et al. Water- and acid-sensitive Cu_2O@Cu–MOF nano sustained-release capsules with superior antifouling behaviors. *ACS Applied Materials & Interfaces*. 2022;14(1):1910-1920. DOI:10.1021/acsami.1c18288

6. Ashraf PM, Lekshmi NM, Chinnadurai S, Anjitha S, et al. Impact assessment of biofouling resistant nano copper oxide–polyaniline coating on aquaculture cage nets. *Aquaculture and Fisheries*. 2023;8(5):538-543. DOI:10.1016/j.aaf.2022.01.002

7. Wang N, Zhang R, Liu K, Zhang Y, et al. Application of nanomaterials in antifouling: a review. *Nano Materials Science*. 2024;6(6):672-700. DOI:10.1016/j.nanoms.2024.01.009

8. Mohd Salleh NK, Aziz F, Mohtar SS, Mohammad AM, et al. Strategies to improve the

antimicrobial properties of metal-oxide based photocatalytic coating: a review. *Progress in Organic Coatings*. 2024;187:108183. DOI:10.1016/j.porgcoat.2023.108183

9. Ismael M, Wark M. A simple sol-gel method for the synthesis of Pt co-catalyzed spinel-type $CuFe_2O_4$ for hydrogen production; the role of crystallinity and band gap energy. *Fuel*. 2024;359:130429. DOI:10.1016/j.fuel.2023.130429

10. Udhaya PA, Ahmad A, Meena M, Queen MAJ, et al. Copper ferrite nanoparticles synthesised using a novel green synthesis route: structural development and photocatalytic activity. *Journal of Molecular Structure*. 2023;1277:134807. DOI:10.1016/j.molstruc.2022.134807

11. Kurian J, Jacob Mathew M. A facile approach to the elucidation of magnetic parameters of $CuFe_2O_4$ nanoparticles synthesized by hydrothermal route. *Journal of Magnetism and Magnetic Materials*. 2017;428:204-212. DOI:10.1016/j.jmmm.2016.12.027

12. Hatami K, Baghbantaraghdari Z, Jamaledin D, Dabbagh Moghaddam F, et al. Synthesis characterization antioxidant and antibacterial activities of zinc ferrite and copper ferrite nanoparticles. *Materials Chemistry Horizons*. 2023;2(1):49-56. DOI:10.22128/mch.2022.613.1030

13. Glazkova EA, Bakina OV, Rodkevich NG, Mosunov AA, et al. Copper ferrite/copper oxides (I, II) nanoparticles synthesized by electric explosion of wires for high performance photocatalytic and antibacterial applications. *Materials Science and Engineering: B*. 2022;283:115845. DOI:10.1016/j.mseb.2022.115845

14. Shweta GM, Naik LR, Pujar RB, Matad SN, et al. Cobalt, copper and magnesium doped nickel zinc nanoferrites by solution-combustion method: structural, antibacterial and antifungal properties. *Journal of Metastable and Nanocrystalline Materials*. 2024;39:21-36. DOI:10.4028/p-zan6nS

15. Jaafar RS, Hammood AY. Antibacterial activity and cytotoxicity of spinel copper ferrite nanoparticles synthesized by using sol gel technique and lemon juice as substrate. *Pollution*. 2024;10(1):63-72. DOI:10.22059/poll.2023.361453.1967

16. Dabagh S, Haris SA, Isfahani BK, Ashammakhi N, et al. Zeolite-copper ferrite nanocomposites with improved antibacterial activity and reusability for biomedical applications. *ACS Applied Nano Materials*. 2023;6(22):21412-21423. DOI:10.1021/acsanm.3c05003

17. Makofane A, Motaung DE, Hintsho-Mbita NC. Green synthesis of silver deposited on copper ferrite nanoparticles for the photodegradation of dye and antibiotics. *Applied Surface Science Advances*. 2024;21:100601. DOI:10.1016/j.apsadv.2024.100601

18. Ivanova LYu, Bakina OV, Glazkova YeA, Svarovskaya NV, et al. Safety assessment of the use of bicomponent copper oxide/copper ferrite nanoparticles as antifouling components. *Tekhnologii bezopasnosti zhiznedeyatel'nosti*. 2024;7:53-58. DOI:10.17223/29491665/7/7 (In Russ.)

19. Redfern J, Cunliffe AJ, Goeres DM, Azevedo NF, et al. Critical analysis of methods to determine growth, control and analysis of biofilms for potential non-submerged antibiofilm surfaces and coatings. *Biofilm*. 2024;7:100187. DOI:10.1016/j.bioflm.2024.100187

20. Bakina OV, Glazkova EA, Svarovskaya NV, Rodkevich NG, et al. “Janus”-like Cu-Fe bimetallic nanoparticles with high antibacterial activity. *Materials Letters*. 2019;242:187-190. DOI:10.1016/j.matlet.2019.01.105

21. Bakina O, Pikuschak E, Prokopchuk A, Evplonova E, et al. Enhanced biocidal activity of heterophase zinc oxide/silver nanoparticles contained within painted surfaces. *Coatings*. 2024;14(2):241. DOI:10.3390/coatings14020241

22. Bakina O, Glazkova E, Pervikov A, Lozhkomoev A, et al. Design and preparation of silver–copper nanoalloys for antibacterial applications. *Journal of Cluster Science*. 2021;32(3):779-786. DOI:10.1007/s10876-020-01844-1

23. Trofimov YeA, Mikhaylov GG. Thermodynamic analysis of the Si–Fe–O system at temperatures of 1100-1300 °C. *Izvestiya Chelyabinskogo nauchnogo tsentra UrO RAN*. 2002;1:21-30. (In Russ.)

24. Atacan K. $CuFe_2O_4$/reduced graphene oxide nanocomposite decorated with gold nanoparticles as a new electrochemical sensor material for L-cysteine detection. *Journal of Alloys and Compounds*. 2019;791:391-401. DOI:10.1016/j.jallcom.2019.03.303

25. Bukhtiyarov VI, Kaichev VV, Prosvirin IP. X-ray photoelectron spectroscopy as a tool for in-situ study of the mechanisms of heterogeneous catalytic reactions. *Topics in Catalysis*. 2005;32(1-2):3-15. DOI:10.1007/s11244-005-9254-3

26. Poulston S, Parlett PM, Stone P, Bowker M. Surface oxidation and reduction of CuO and Cu_2O studied using XPS and XAES. *Surface and Interface Analysis*. 1996;24(12):811-820. DOI:10.1002/(SICI)1096-9918(199611)24:12<811::AID-SIA191>3.0.CO;2-Z

27. Wollner A, Lange F, Schmelz H, Knozinger H. Characterization of mixed copper-manganese oxides supported on titania catalysts for selective oxidation of ammonia. *Applied Catalysis A: General*. 1993;94(2):181-203. DOI:10.1016/0926-860X(93)85007-C

28. Qin Q, Liu Y, Li X, Sun T, et al. Enhanced heterogeneous fenton-like degradation of methylene blue by reduced $CuFe_2O_4$. *RSC Advances*. 2018;8(2):1071-1077. DOI:10.1039/C7RA12488K

29. Ranathunga K, Yapa P, Munaweera I, Weerasekera MM, et al. Preparation and characterization of Fe–ZnO cellulose-based nanofiber mats with self-sterilizing photocatalytic activity to enhance antibacterial applications under visible light. *RSC Advances*. 2024;14(26):18536-18552. DOI:10.1039/D4RA03136A

30. Harja M, Buema G, Bucur D. Recent advances in removal of Congo red dye by adsorption using an industrial waste. *Scientific Reports*. 2022;12(1):6087. DOI:10.1038/s41598-022-10093-3

31. Sudarsan S, Anandkumar M, Trofimov EA. Synthesis and characterization of copper ferrite nanocomposite from discarded printed circuit boards as an effective photocatalyst for Congo red dye degradation. *Journal of Industrial and Engineering Chemistry*. 2024;131:208-220. DOI:10.1016/j.jiec.2023.10.020

32. Kirankumar VS, Hardik B, Sumathi S. Photocatalytic degradation of Congo red using copper substituted cobalt ferrite. *IOP Conference Series:*

Materials Science and Engineering. 2017;263:022027. DOI:10.1088/1757-899X/263/2/022027

33. Akhter M, Amin MdK, Dhar PK, Dey SK, et al. Fabrication of rare-earth cerium-doped nickel-copper ferrite as a promising photo-catalyst for Congo red-containing wastewater treatment. *RSC Advances*. 2024;14(40):29083-29098. DOI:10.1039/D4RA04334K

34. Mosabberul Haque Md, Rahman A, Shafiul Islam Shahin Md, Ahsan Habib Md, et al. Manganese doped copper ferrite nanoparticles: a promising approach for organic dye elimination under light irradiation. *Results in Chemistry*. 2024;7:101509. DOI:10.1016/j.rechem.2024.101509

35. Selmi A, Teymourinia H, Zarei A, Timoumi M, et al. CMCFO-$Cr_{0.1}$ nanoferrites: sol-gel synthesis structural and magnetic studies: applications for photodegradation of Congo red dye. *Iranian Journal of Catalysis*. 2022;12(1):97-106. DOI:10.30495/ijc.2022.689626

36. Hussain M, El Sayed ME, Anwar M, Samir A, et al. Influence of transition metal (Cu) and rare earth metal (Dy) co-doping on spinel zinc ferrite ($Cu_{0.1}Dy_{0.08}Zn_{0.9}Fe_{1.92}O_4$) for improved photocatalytic degradation of industrial effluents. *Journal of Alloys and Compounds*. 2025;1010:177242. DOI:10.1016/j.jallcom.2024.177242

37. Afaq M, Basha B, Warsi MF, Shahid M, et al. Fabrication of ZnO–$CuFe_2O_4$–CNTs ternary nanocomposite for harmful organic effluents degradation by sunlight irradiation. *Materials Science and Engineering: B*. 2023;292:116444. DOI:10.1016/j.mseb.2023.116444

38. Oliveira TP, Rodrigues SF, Marques GN, Viana Costa RC, et al. Synthesis, characterization, and photocatalytic investigation of $CuFe_2O_4$ for the degradation of dyes under visible light. *Catalysts*. 2022;12(6):623. DOI:10.3390/catal12060623

Information about the authors / Информация об авторах

Ekaterina A. Vornakova, Junior Researcher, Institute of Strength Physics and Materials Science of Siberian Branch Russian Academy of Sciences, Tomsk, Russian Federation; ORCID 0000-0003-2930-4932; e-mail: katya.vornakova@mail.ru

Valeria R. Chzhou, Junior Researcher, Institute of Strength Physics and Materials Science of Siberian Branch Russian Academy of Sciences, Tomsk, Russian Federation; ORCID 0000-0001-9610-1161; e-mail: chzhou.vr@ispms.ru

Olga V. Bakina, D. Sc. (Eng.), Leading Researcher, Institute of Strength Physics and Materials Science of Siberian Branch Russian Academy of Sciences, Tomsk, Russian Federation; ORCID 0000-0002-8650-6939; e-mail: ovbakina@ispms.ru

Ludmila Yu. Ivanova, Cand. Sc. (Eng.), Research Fellow, Institute of Strength Physics and Materials Science of Siberian Branch Russian Academy of Sciences, Tomsk, Russian Federation; ORCID 0000-0003-1953-307x; e-mail: ivanova_lu@ispms.ru

Anastasia E. Yafaeva, PhD Student, Institute of Strength Physics and Materials Science of Siberian Branch Russian Academy of Sciences, Tomsk, Russian Federation; ORCID 0009-0005-2115-0440; e-mail: yafaeva98@mail.ru

Marat I. Lerner, D. Sc. (Eng.), Head of the Laboratory, Institute of Strength Physics and Materials Science of Siberian Branch Russian Academy of Sciences, Tomsk, Russian Federation; ORCID 0000-0001-8565-1344; e-mail: lerner@ispms.ru

Ворнакова Екатерина Андреевна, младший научный сотрудник, Институт физики прочности и материаловедения СО РАН, Томск, Российская Федерация; ORCID 0000-0003-2930-4932; e-mail: katya.vornakova@mail.ru

Чжоу Валерия Романовна, младший научный сотрудник, Институт физики прочности и материаловедения СО РАН, Томск, Российская Федерация; ORCID 0000-0001-9610-1161; e-mail: chzhou.vr@ispms.ru

Бакина Ольга Владимировна, доктор технических наук, ведущий научный сотрудник, Институт физики прочности и материаловедения СО РАН, Томск, Российская Федерация; ORCID 0000-0002-8650-6939; e-mail: ovbakina@ispms.ru

Иванова Людмила Юрьевна, кандидат технических наук, научный сотрудник, Институт физики прочности и материаловедения СО РАН, Томск, Российская Федерация; ORCID 0000-0003-1953-307x; e-mail: ivanova_lu@ispms.ru

Яфаева Анастасия Эдуардовна, аспирант, Институт физики прочности и материаловедения СО РАН, Томск, Российская Федерация; ORCID 0009-0005-2115-0440; e-mail: yafaeva98@mail.ru

Лернер Марат Израильевич, доктор технических наук, заведующий лабораторией, Институт физики прочности и материаловедения СО РАН, Томск, Российская Федерация; ORCID 0000-0001-8565-1344; e-mail: lerner@ispms.ru

Received 20 March 2025; Revised 29 April 2025; Accepted 07 May 2025